Influence of surface-mode-enhanced local fields on photophoresis

S. Arnold
Institute for Imaging Sciences and Department of Physics, Polytechnic Institute of New York, 333 Jay Street, Brooklyn, New York 11201

A. B. Pluchino
Infrared Space Optics Section, Chemistry and Physics Laboratory, The Aerospace Corporation, P. O. Box 92957, Los Angeles, California 90009

K. M. Leung
Department of Physics, Polytechnic Institute of New York, 333 Jay Street, Brooklyn, New York 11201
(Received 9 September 1983)

The radiometric force (photothermal) on a sphere is investigated theoretically in the surface-mode region ($-1>\epsilon>-2$). Closed-form expressions obtained for this force in the transition regime ($K_n \sim 1$) reveal a quasi-double-resonant character, with contributions from both dipole and quadrupole surface modes. Full Mie calculations verify these asymptotic expressions and extend the range of the calculations to an optical size (the ratio of the circumference to the wavelength) near 1. Applications of the theory to surface plasmons in Ag and surface phonons in SiC show that excitation of the quadrupole mode causes a reversal in the radiometric force with a factor-of-10^4 increase in magnitude. The overall force (radiometric plus radiation pressure) is evaluated, and photophoretic spectra are presented.

I. INTRODUCTION

Recently, there has been a great deal of interest in phenomena associated with the huge fields which can be produced on the surface of small particles from the stimulation of surface modes. Thus Raman scattering from adsorbed molecules on rough surfaces[1,2] and photoemission from small aerosol particles are found[3] to be enhanced by orders of magnitude in materials which demonstrate surface modes in the visible and near uv. Silver apparently shows the largest effects. Years ago, a number of interesting phenomena were discovered associated with photophoresis on silver.[4]

In experiments on light-induced motion of Ag particles of ~ 1000 Å radius in a N_2 atmosphere, a fraction of the particles was observed to move backward toward the light source. The experimenters[4] reasoned that this behavior was anomalous since photophoresis was thought to be due to increased momentum transport into the external gas as a result of surface heating; they could not understand how the most highly reflecting material could be heated most at its back surface. In what follows, we theoretically investigate the internal field distribution of a small particle near a surface-mode resonance. We will show in apparent contradiction to common sense that the electromagnetic field may be greatest at the back surface when the stimulating radiation is in the region of a surface-mode resonance, and that under these conditions, although the particle is small compared to the wavelength, the Rayleigh theory is not applicable. The electric response near the surface plasmon and phonon modes in Ag and SiC, respectively, are used as examples, and their respective radiometric forces are calculated.

II. THEORY

The history of theories of photophoresis is extensive.[5] For the most part up until 1982,[6] calculations for specific materials were not made. The lack of interest almost certainly stems from the lack of experiments on well-characterized particles and the difficulty associated with doing extensive numerical calculations. With the invention of a photophoretic spectrometer[7,8] this trend has reversed. Recently Pluchino[9] has shown that photophoretic spectra of glycerol[10] may be modeled and although his calculations only appear to give the magnitude of the force within a factor of ~ 2, they do reveal the sign of the force and specific structure which is seen in the size spectrum. The particular model from which Pluchino calculated was that of Yalamov *et al.*[11] It is a model which deals with photophoresis at low Knudsen number (gas mean free path λ is much less than the particle radius R). As the Knudsen number is increased corrections for the breakdown of continuum hydrodynamics must be included. Recently this Knudsen number dependence was incorporated in the calculations of Pluchino, resulting in a comprehensive theory[12] that reproduces the experimental data to within the experimental error of 5%.

In the limit of low Knudsen number, a surface temperature gradient $\vec{\nabla} T_s$ causes molecules at the surface to undergo a motion in the direction of the gradient known as "Maxwellian creep."[13] At the surface of a sphere, this creep velocity is given by

$$V_\theta = \frac{K\eta_e}{RT_s\rho_g}\frac{\partial T_s}{\partial \theta}\ , \tag{1}$$

where K is the coefficient of thermal slip[14] (a number be-

tween 0.7 and 1.5), T_s is the surface temperature, R is the particle radius, ρ_g is the density of the external gas, η_e is the gas viscosity, and angle θ is defined in Fig. 1. The stress imparted to the gas by the unevenly heated surface produces a reaction on the surface which is the origin of the radiometric force (photothermal) in the small Knudsen number regime. Yalamov *et al.*[11] have shown by applying such a stress to the surface that the resulting force $\vec{F}_r$ is

$$\vec{F}_r = -\frac{4\pi R \eta_e^2 J K \vec{I}}{\rho_g T_s K_i} , \tag{2}$$

where K_i is the interior thermal conductivity, $\vec{I}$ is the incident intensity, and J is a measure of the asymmetry of the internal heat sources. This asymmetry factor is actually a composite of two dimensionless factors, the well-known absorption efficiency Q_a and an anisotropy factor A_z, $J = \frac{3}{8} Q_a A_z$.[10] This anisotropy factor which provides a measure for the distribution of the absorbed energy is given by

$$A_z = \frac{\int_0^1 dx' x'^3 \int_0^\pi d\theta \sin(2\theta) \, |\vec{E}_i(x',\theta)|^2}{\int_0^1 dx' x'^2 \int_0^\pi d\theta \sin\theta \, |\vec{E}_i(x',\theta)|^2} , \tag{3}$$

where x' is the dimensionless length r/R and $|E_i(x',0)|^2$ is the square modulus of the internal electric field strength averaged over the azimuthal angle ϕ. It is A_z which controls the sign of the force; with A_z positive, the back surface is heated most effectively and the particle moves back toward the light source (negative photophoresis). In what follows we will investigate the internal field for optically small particles. Our description follows that of Van de Hulst.[15]

The components of $\vec{E}$ and $\vec{H}$ are written as

$$\begin{aligned} \vec{E} &= \vec{M}_v + i\vec{N}_u , \\ \vec{H} &= m(-\vec{M}_u + i\vec{N}_v) , \end{aligned} \tag{4}$$

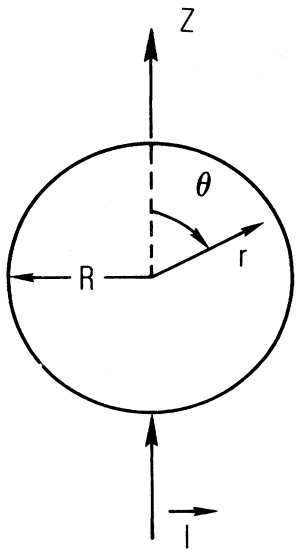

FIG. 1. Coordinate system used in evaluating Eq. (3).

where m is the refractive index ($m = n_r + ik$) and where the derived vector fields $\vec{M}$ and $\vec{N}$ are defined by

$$\begin{aligned} \vec{M}_\Psi &= \vec{\nabla} \times (\vec{r}\Psi) , \\ mk\vec{N}_\Psi &= \vec{\nabla} \times \vec{M}_\Psi , \end{aligned} \tag{5}$$

with Ψ (u or v) a solution of the scalar wave equation. Within the sphere u and v are given by

$$\begin{aligned} u &= e^{i\omega t}\cos\phi \sum_{n=1}^{\infty} m c_n (-i)^n \frac{(2n+1)}{n(n+1)} P_n^i(\cos\theta) j_n(mkr) , \\ v &= e^{i\omega t}\cos\phi \sum_{n=1}^{\infty} m d_n (-i)^n \frac{(2n+1)}{n(n+1)} P_n^i(\cos\theta) j_n(mkr) , \end{aligned} \tag{6}$$

where P_n is the associated Legendre polynomial, j_n is the spherical Bessel function, $k = 2\pi/\lambda$, and c_n and d_n, which are determined by matching boundary conditions at the surface of the sphere, are given by

$$c_n = i[\Psi_n'(y)\zeta_n(x) - m\Psi_n(y)\zeta_n'(x)]^{-1}$$

and

$$d_n = i[m\Psi_n'(y)\zeta_n(x) - \Psi_n(y)\zeta_n'(x)]^{-1} , \tag{7}$$

with $x = kR$, $y = mx$, $\Psi_n(z) = (\pi z/2)^{1/2} J_{n+1/2}(z)$, and $\zeta_n(z) = (\pi z/2)^{1/2} H_{n+1/2}^{(2)}(z)$. $J_{n+1/2}$ and $H_{n+1/2}^{(2)}$ are the Bessel functions of the first and second kind, respectively. In the limit of small optical size, $x \ll 1$ and $|y| \ll 1$, the functions Ψ_n, Ψ_n', ζ_n, and ζ_n' may be represented using series expansions. This approach provides us with the following expressions for c_n and d_n to first order in x,

$$\begin{aligned} c_n &= \frac{(2n+1)e^{ix}}{m^n(m^2 n + n + 1)}(1 - ix) , \\ d_n &= \frac{e^{ix}}{m^{n+1}}(1 - ix) . \end{aligned} \tag{8}$$

It is important to note that although d_n is well behaved as a function of m, c_n has resonances at frequencies ω_n such that

$$m^2 + (n+1)/n = 0, \quad n = 1,2,3,\ldots . \tag{9}$$

The lowest-order mode $m^2 = -2$ corresponds to the well-known electric dipole surface-mode resonance which is apparent in extinction in Ag at 355 nm (see Ref. 16) and in SiC at 10.72 μm.[17] The higher-order surface-mode resonance ($n = 2$) is an electric quadrupole. This mode which resonates in Ag at 347 nm (see Ref. 16) and in SiC at 10.63 μm (see Ref. 17) is not seen in small-particle extinction experiments but will be of principle importance in controlling the anisotropy [Eq. (3)] in photophoresis. The contribution of higher-order modes to the internal field structure is muted in Eq. (6), by the rapid falloff with size demonstrated by $j_n(mkr)$. Since this function falls off as $(mkr)^n$, for arguments considerably less than 1, terms higher than $n = 2$ should be relatively unimportant and are not considered in the present analysis.

The electric fields within the sphere can then be written down to first order in x. We have

$$E_r=\pi^{1/2}mie^{i\omega t}\cos\phi\left[\frac{\gamma_1 c_1}{2\Gamma(5/2)}\sin\theta+\frac{9(mkr)\gamma_2 c_2}{4\Gamma(7/2)}\sin\theta\cos\theta\right]E_0\,,$$

$$E_\theta=\pi^{1/2}me^{i\omega t}\cos\phi\left[\frac{i\gamma_1 c_1}{2\Gamma(5/2)}\cos\theta+\frac{9i(mkr)\gamma_2 c_2}{8\Gamma(7/2)}\cos(2\theta)+\frac{(mkr)\gamma_1 d_1}{4\Gamma(5/2)}\right]E_0\,, \tag{10}$$

$$E_\phi=-\pi^{1/2}me^{i\omega t}\sin\phi\left[\frac{i\gamma_1 c_1}{2\Gamma(5/2)}+\frac{9(mkr)\gamma_2 c_2\cos\theta}{8\Gamma(7/2)}+\frac{(mkr)\gamma_1 d_1\cos\theta}{4\Gamma(5/2)}\right]E_0\,,$$

where $\gamma_n=i^n(2n+1)/n(n+1)$, E_0 is the electric field amplitude of the incident radiation (polarized in the $\phi=0$ plane), and $\Gamma(x)$ is the gamma function.

One can clearly see the dipole character in the first term in E, whereas this term is associated with two nodes in E_θ in π radians. The next term which goes as $\cos(2\theta)$ has four nodes, a quadrupole. Figure 2 shows a drawing of these modes for $\phi=0$. This figure is similar to drawings presented by Mie[18] with the exception that in the present case the particle is shown inscribed within the charges making up each multipole. Near the surface-mode region, $-2<m^2<-1$, the dipole and quadrupole terms are dominant in E. We have drawn Fig. 2 so that the phase relationship between these terms is similar to that which would exist in the surface-quadrupole region (near $m^2\sim-\frac{3}{2}$). One sees that the vector sum of the fields in Fig. 2 produces a larger field at the back of the particle than at the front. This polarization of the internal heat sources is more apparent in $|E(r,\theta)|^2$ which is found by combining Eq. (10) to form $|E(r,\theta,\phi)|^2$ and then averaging over ϕ. This so-called "source function" is then

$$|E(r,\theta)|^2=\frac{9E_0^2}{|m^2+2|^2}\times\left[1-\tfrac{2}{3}n_r Kkr\cos\theta\left[1-\frac{5}{|2m^2+3|^2}\right]\right]. \tag{11}$$

Equation (11) agrees with the approximate result reported by Yalamov *et al.*[19] The authors concluded that more heat will be evolved on the illuminated side of a particle, however, once again we see that the back to front polarization of heat sources can be reversed if the fraction $5/|2m^2+3|^2$ is greater than 1. In almost all dielectric materials, this is not the case; however, near-surface-mode resonances $5/|2m^2+3|^2$ may be considerably greater than 1. For example, based on refractive index data for SiC (see Ref. 17) at 10.63 μm, $5/|2m^2+3|^2=39.2$. A similar reversal in the heat-source polarization is found in Ag at 347 nm. Using Eqs. (11) and (3), we arrive at an expression for the asymmetry factor J,

$$J=\frac{3}{8}\left[-\frac{12x\epsilon''(\omega)}{|\epsilon(\omega)+2|^2}\right]\times\left[-\frac{2x}{15}\epsilon''(\omega)\left[\frac{5/4}{|\epsilon(\omega)+3/2|^2}-1\right]\right], \tag{12}$$

where $\epsilon=m^2$ and $\epsilon''=\mathrm{Im}\epsilon$. This expression has been factored so that the first term is the absorption efficiency Q_a and the second term is the anisotropy factor A_z. Since the radiometric force and J are proportional to each other, the spectral dependence of J is the spectrum of this force. Note that the resonance in A_z at $\epsilon=-\frac{3}{2}$ is of little consequence in the radiometric force unless it is also accompanied by near-resonance conditions in Q_a. As we will see below, this quasi-double-resonance situation is borne out for the following examples.

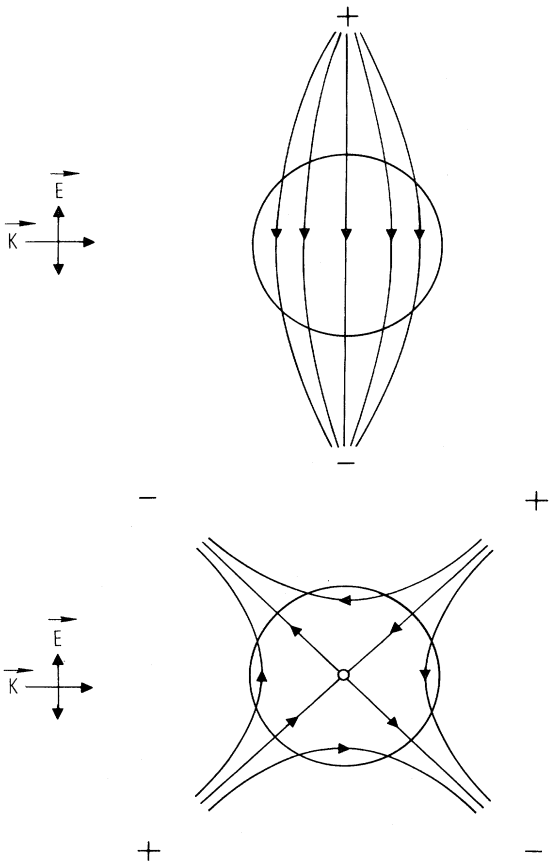

FIG 2. Electric lines of force for the dipole and quadrupole modes. The relative phases shown are similar to the situation existing at the quadrupole resonances in Figs. 3 and 6.

III. CALCULATIONS

A. Ionic solids

Collective oscillations of lattice ions in solids lead to phonon modes. The dielectric response in the region of

these modes is given by

$$\epsilon(\omega)=\epsilon_\infty+\frac{\omega_p^2}{\omega_t^2-\omega^2-i\gamma\omega}\ , \tag{13}$$

where ω_p is the plasmon frequency associated with the lattice ions, and ω_t is the transverse-optical-mode frequency. Unlike the plasmon frequency associated with electrons in a metal, which is found in the ultraviolet, the phonon dispersion in Eq. (13) corresponds to a plasmon frequency in the ir. This much smaller frequency is due primarily to the significantly large mass of lattice ions compared with free electrons. A good example of a material which follows the dispersion in Eq. (13) is SiC,[17] for which $\omega_p=1441$ cm^{-1}, $\omega_t=794$ cm^{-1}, $\epsilon_\infty=6.7$, and $\gamma=5.6$ cm^{-1}. Figure 3 shows the factors Q_a, A_z, and J calculated from Eq. (12) in the region of the surface-mode resonances for a particle with a radius of 0.34 μm ($x=0.2$ at the quadrupole resonance). We see that although Q_a demonstrates a resonance at 932 cm^{-1}, the factor A_z is peaked nearby at 941 cm^{-1}. These energies correspond, respectively, to the surface dipole and quadrupole resonances. Although the radiometric force is forward at 970 cm^{-1}, the force reverses as the energy is reduced below 954 cm^{-1} and climbs in magnitude so that the maximum reversed value at 941 cm^{-1} is 10^3 times the value at 970 cm^{-1}. This dramatic increase in the radiometric force due to the nearly simultaneous excitation of dipole and quadrupole modes is surprising in as much as the usual criteria for the use of Rayleigh theory[20] (dipole resonance only, $R/\lambda<0.05$) is easily met in the present case. In light of this disparity we felt it was necessary to perform a full Mie calculation of the internal field in order to check the validity of our approximate result [Eq. (12)]. Figure 4(b) shows an internal source distribution $|\vec{E}(\vec{r})|^2$ for a SiC particle having a size parameter of 0.2 at 941 cm^{-1}. This diagram represents an equatorial slice through the particle, and clearly shows the sources polarized toward the back. Figure 4(a) is a calculation on the same particle at 970 cm^{-1}. Relative to Fig. 4(a) this particle has essentially no asymmetry in internal field sources. The number at the top of Fig. 4(a) is the ratio of the square modulus of the field at the far side (back) of the sphere to the square modulus of the field of the incident radiation. A comparison of this number with that in Fig. 4(b) shows that a great deal more absorption takes place at 941 cm^{-1} than at 970 cm^{-1}. Figure 4(c) is a calculation at 941 cm^{-1} for a size parameter of 0.6. The internal sources clearly do not simply increase linearly with z (i.e., $z=r\cos\theta$) as required by Eq. (11). However, we still see the backward polarization of the sources. Figure 5 shows a comparison of the approximate J factor as calculated from Eq. (12) with the result of the full Mie calculation for an energy of 941 cm^{-1} in SiC. Equation (11) is found to be accurate to within 15% for $x<0.2$. In addition, the largest reversed effect for the energy is reached at $x\sim0.5$.

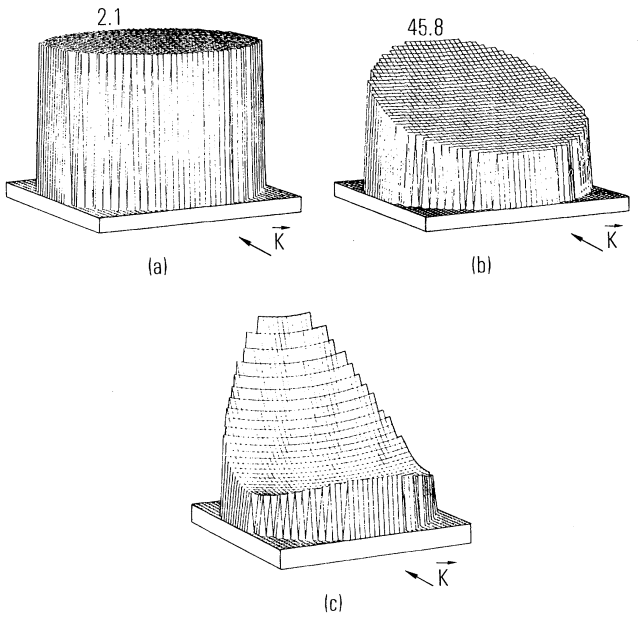

FIG. 4. Vertical displacement is the source strength $|E(r,\theta)|^2/|E_0|^2$, where $|E_0|^2$ is the square modulus of the field strength in the incident beam. This source function is pictured within an equatorial slice perpendicular to the incident vertical polarization. The direction of the incident radiation is indicated by $\vec{K}$. The round perimeter near the base in each picture is the perimeter of the particle. In (a) and (b) the particle with $x=0.2$ is SiC at 970 and 941 cm^{-1}, respectively. In (c) a SiC particle with $x=0.6$ is irradiated at 941 cm^{-1}.

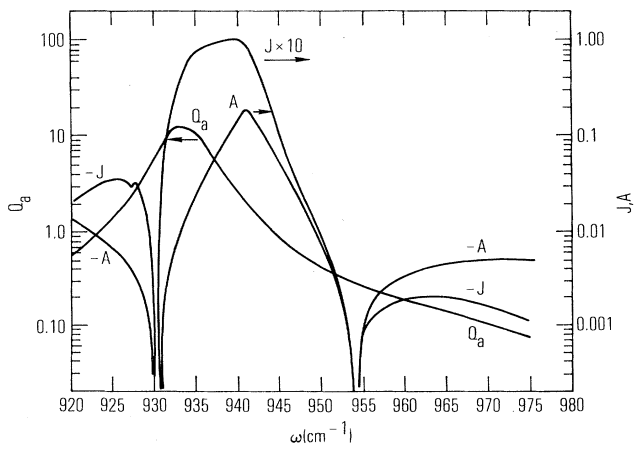

FIG. 3. Factors Q_a, A_z, and J vs energy ω as calculated from Eq. (12) for SiC (see Ref. 17) with $R=0.34$ μm.

B. Metals

In free-electron metals the dielectric function is expected to follow the Drude formula

$$\epsilon(\omega)=1-\frac{\omega_p^2}{\omega^2+i\gamma\omega}\ , \tag{14}$$

where ω_p is the plasmon frequency of the electron and γ is a damping coefficient. As long as γ is a small frequency with respect to ω_p, ω will reach the surface-dipole reso-

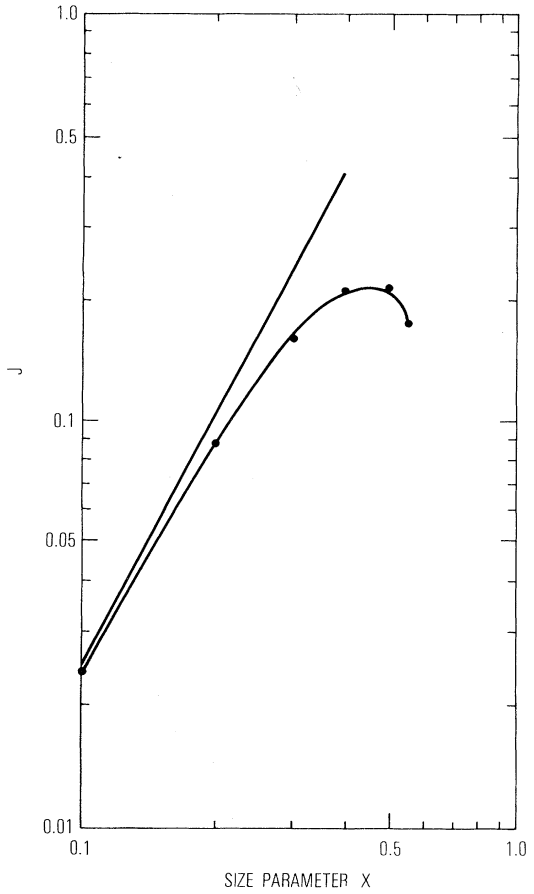

FIG. 5. Comparison for SiC between J as calculated from Eq. (12) (solid line) and a full Mie calculation, for energy $\omega=941$ cm^{-1}.

nance ($\epsilon=-2$) at $\omega_p/\sqrt{3}$ and the surface-quadrupole resonance at the slightly higher frequency $\omega_p/(\sqrt{5/2})$. As Johnson and Christy[16] have observed, Ag is not a free-electron metal; however, the relative positions of the quadrupole and dipole resonances are preserved. Using the refractive index data given in Ref. 16, we have calculated Q_a, A_z, and J from Eq. (12) near the surface-mode region in the near ultraviolet. Figure 6 shows these calculations. A comparison of Fig. 6 with Fig. 3 shows that the features in the silver spectrum are qualitatively similar to those found in SiC. Again a large reversed force is produced with a maximum value near the quadrupole resonance. This resonance is reached in Ag at 355 nm. A complete Mie calculation reveals that J has a maximum value for 355-nm light of 0.23 at a size x of 0.5. Beyond this size the force drops off rapidly so that J at $x=1$ is 0.068. We are now in a position to calculate the overall force on both SiC and Ag.

C. Overall force

In the presence of a gas, the overall force $\vec{F}$ on a particle has several parts,

$$\vec{F}=\vec{F}_r+\vec{F}_p\ , \tag{15}$$

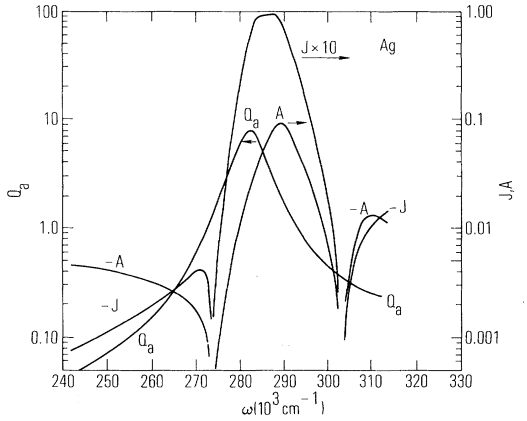

FIG. 6. Factors Q_a, A_z, and J vs energy ω as calculated from Eq. (12) for Ag (see Ref. 16) with $R=113$ Å.

where $\vec{F}_r$ is the radiometric component due to the thermal stimulation of gas dynamic modes and $\vec{F}_p$ is the force due to radiation pressure. We assume here that impulses caused by inelastic scattering (e.g., Raman, fluorescence) and thermal reradiation are unimportant in the present case, so that Debye's result

$$\vec{F}_p=\frac{1}{c}[Q_a+Q_s(1-\langle\cos\theta\rangle)]\pi R^2\vec{I} \tag{16}$$

is applicable.[21] The expression $Q_s(1-\langle\cos\theta\rangle)/c$ represents the scattered intensity contribution to the force ($\langle\cos\theta\rangle$ is the elastic scattering asymmetry factor). The radiometric force $\vec{F}_r$ as obtained from Eq. (2) only applies in the case of low Knudsen number. Since the largest radiometric forces occur when the mean free path λ and particle radius are comparable, for a significant radiometric component we should modify Eq. (2). Within the transition regime it has been shown[12,22] that an adequate approximation is obtained by multiplying Eq. (2) by

$$g(K_n)=\frac{1}{1+3C_mK_n}\frac{1}{1+2C_tK_n}\ , \tag{17}$$

where C_m is related to momentum accommodation at the gas-particle interface (a number between 1.00 and 1.35) and C_t is the temperature jump coefficient (a number between 1.875 and 2.48).[23] Combining Eqs. (17) and (2), and the definition of J, we arrive at

$$\vec{F}_r=-\left[\frac{3}{2}\frac{\eta^2F(K_n)}{\lambda_0\rho_0T_sK_i}\right]\left[A_zQ_a\pi R^2\vec{I}\ \right]\ , \tag{18}$$

where $F(K_n)$ is $K_ng(K_n)$ and we have utilized the inverse relationship between λ (the mean free path) and ρ_g for a dilute gas (i.e., $\rho_g=\rho_0\lambda_0/\lambda$, where ρ_0 and λ_0 are the density and mean free path at 1 atm). The first quantity in large parentheses in Eq. (18), which we will label B, contains only thermal and gas dynamic information. One can ask where this quantity will be optimum with pressure. The answer clearly is the point at which the function $F(K_n)$ is optimum. For reasonable values of C_m and C_t the optimal value of $F(K_n)$ corresponds to a Knudsen

number of ~ 0.25 and lies between 0.050 and 0.075.[22] With this form for the radiometric force [Eq. (18)], the overall force from Eqs. (15), (16), and (18) becomes

$$\vec{F}=\frac{1}{c}[Q_a(1-cBA_z)+Q_s(1-\langle\cos\theta\rangle)]\pi R^2\vec{I} \ . \quad (19)$$

For a small particle ($x<0.1$), $Q_s/Q_a \ll 1$ and we see in this limit that the sign of the force has nothing to do with the amount of heat absorbed (i.e., the sign only depends on A_z, thermal and gas dynamic properties). Figure 7 shows the photophoretic spectrum F/mg (mg in the gravitational force) vs ω for a particle of SiC with a radius of 0.34 μm ($x\sim 0.2$) in a field of radiation with an intensity of 10^4 W/cm^2. An optimal value for $F(K_n)$ of 0.060 was chosen ($K_n\sim 0.25$, pressure ~ 0.7 atm) and a bulk thermal conductivity has been assumed (K_i for SiC is taken to be 2.5 W/cm K).[24] To place this figure in perspective it should be pointed out that the thermal conductivity of SiC (see Ref. 24) is only slightly less than that of Ag, and therefore, the particle is practically a thermal short. The result for a perfect thermal short (i.e., $K_i=\infty$) is shown in the upper curve in Fig. 7; the middle curve shows the result for the reported thermal conductivity of SiC, and the lowest curve represents a particle having the same optical properties of SiC but with $\frac{1}{3}$ the thermal conductivity. We clearly see in the case of SiC (middle curve) that both the dipole and quadrupole resonances are apparent. The dipole shows up as a forward force at 932 cm^{-1}, and the quadrupole which resonates near 941 cm^{-1} results in a significantly small reversed force. The radiometric component of the force increases relative to the photon pressure as the thermal conductivity of the particle is reduced (lower curve).

A silver particle with an optical size of 0.2 at 350 nm would have a diameter of ~ 280 Å. Based on the current physical model of photophoresis and the similarities between Fig. 3 and 6, a result similar to Fig. 7 for SiC would be produced for Ag in the surface-mode region of Ag (310—400 nm). However, due to a significantly larger thermal conductivity (for a single crystal $K_i=4.3$ W/cm K) and a smaller maximum anisotropy factor, the maximum reversed radiometric force near the quadrupole resonance is less than half the force due to radiation pressure. Thus, according to our model Ag with single-crystal thermal properties cannot show an overall reversed force for a diameter of 280 Å. However, the assumption of diffusive-thermal transport at this size is questionable since in a single crystal the electron mean free path may be several hundred angstroms (300 Å) at room temperature. Consequently, it is necessary to test our conclusion for larger size particles. In fact the early results of Lustig and Sollner[4] on photophoresis of Ag were performed in particles 600—1300 Å in radius in one atm of nitrogen. In Fig. 8, we see the results of a computer intensive calculation performed on a particle with $R=850$ Å in nitrogen at 1 atm [$F(K_n)$ was evaluated by using the same values of C_m and C_t as in the case of SiC]. The ratio of the radiometric force to the radiation pressure force is represented in Fig. 8. We see in this case that the radiometric force grows to within 0.6 of the radiation pressure at ~ 350 nm. A relief diagram of the internal sources at this optimum wavelength (to the left in Fig. 8) shows that the sources are almost all at the back of the particle. Once again we see on the basis of single-crystal thermal conductivity, that Ag will not exhibit reversed photophoresis.

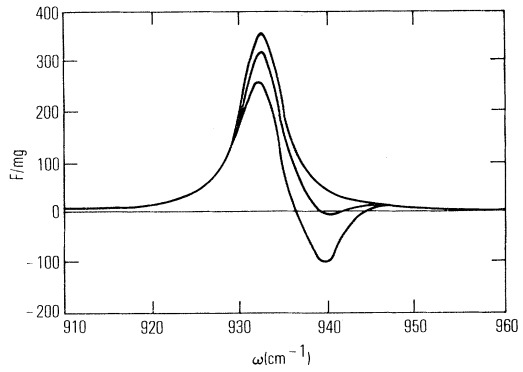

FIG. 7. Simulated photophoretic spectra for SiC particle with $R\sim 0.3$ μm in air at 0.7 atm. The top curve is the result for an infinite thermal conductivity K_i, the center curve is for the value of K_i reported in the literature, and the bottom curve shows the effect of lowering K_i by a factor of 3. The assumed light intensity is 10^4 W/cm^2.

IV. DISCUSSION

In the preceding sections we have investigated the influence of surface modes on photophoresis for the first time.

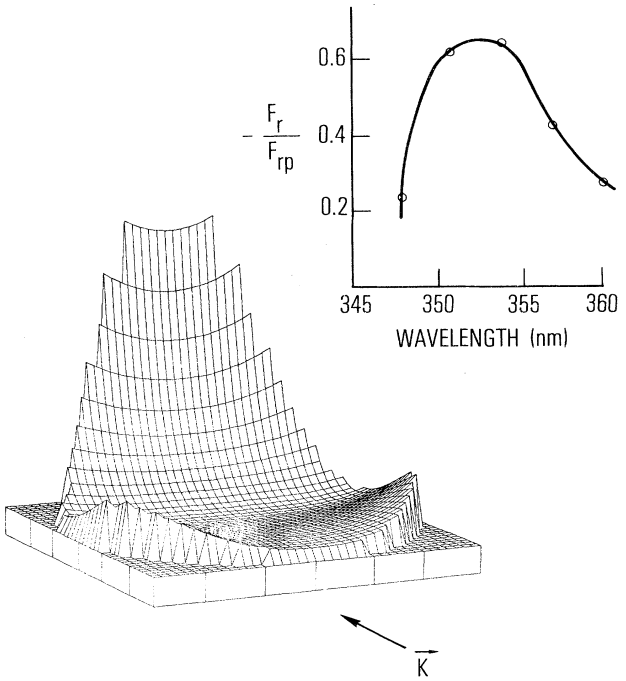

FIG. 8. Source strength relief diagram for a particle of 850 Å radius at an excitation wavelength of 354 nm. The curve at the upper right shows the ratio of the radiometric to radiation pressure force on this particle in N_2 at 1 atm.

Our model assumes diffusive thermal transport within the particle and neglects quantum size effects. Within these assumptions we find the major effect to be of the generation of a reversed radiometric force due primarily to a quasi-double-resonance of dipole and quadrupole modes. The interference between these modes produces a large anisotropy in the internal field in particles whose optical size normally is considered to place them in the Rayleigh range. Although a SiC sphere with $R \sim 0.3$ μm in air (pressure ~ 0.7 atm) is expected to yield a net negative mobility in 10.63-μm radiation, for an Ag sphere having single-crystal-like thermal conductivity, we find no combination of size, pressure, and radiation wavelength which will give rise to a net negative mobility. The principal limitation in Ag is its high thermal conductivity. If the thermal conductivity were reduced to $\frac{1}{2}$ of its bulk value, a net negative mobility would be calculated at 350 nm for a sphere with $R = 850$ Å. However, to produce a net negativity mobility in broadband thermal radiation, as used by Lustig and Sollner,[4] one would have to reduce the thermal conductivity of Ag to unreasonable levels. Therefore, we conclude that the Ag particles seen to move backward[4] were not homogeneous spheres. Recent electron micrographs indicate that particles produced from an exploding wire[25] (a method similar to the arc discharge used in Ref. 4) shows a majority of spherical particles and minority of clusters. We propose that the particles seen to move backward in Ref. 4 were clusters. This proposal is consistent with our calculations and the electron micrographs since the majority of particles observed by Lustig and Sollner[4] demonstrated positive photophoresis. We conclude that photophoretic spectroscopy experiments performed near a structure resonance should be rich in providing information concerning the optical response of individual particles as well as elucidating the mechanisms for internal thermal transport. To our knowledge no other method exists for studying thermal transport within an individual particle of ~ 1000 Å in size.

ACKNOWLEDGMENTS

We would like to thank A. Oliner and A. Zangwill of the Electrical Engineering and Physics Departments (PINY), respectively, for useful discussions. Our thanks also go to Susan Ma of the Microparticle Photophysics Laboratory for help in preparing the original manuscript. This work was supported by a grant from the National Science Foundation (Grant No. ATM-82-08313), to S.A., who was also supported by an Alfred P. Sloan fellowship. K.M.L.'s support was provided by the U.S. Joint Services Electronic Contract No. F49620-80-C-0077, and A.B.P. was supported by The Aerospace Corporation.

[1]T. E. Furtak and J. Reyes, Surf. Sci. 92, 351 (1980).
[2]*Surface Enhanced Raman Scattering,* edited by R. K. Chang and T. E. Furtak (Plenum, New York, 1982).
[3]A. Schmidt-Ott, P. Schurtenberger, and H. C. Siegman, Phys. Rev. Lett. 45, 1284 (1980).
[4]A. Lustig and A. Sollner, Z. Phys. 79, 823 (1932).
[5]O. Preining, in *Aerosol Science,* edited by C. N. Davies (Academic, New York, 1966).
[6]M. Kerker and D. D. Cooke, J. Opt. Soc. Am 72, 1267 (1982).
[7]S. Arnold and Y. Amani, Opt. Lett. 5, 242 (1980).
[8]S. Arnold, Y. Amani, and A. Orenstein, Rev. Sci. Instrum. 51, 1202 (1980).
[9]A. B. Pluchino, Appl. Opt. 22, 103 (1983).
[10]S. Arnold and M. Lewittes, J. Appl. Phys. 53, 5314 (1982).
[11]Yu. I. Yalamov, V. B. Kutukov, and E. R. Suchukin, J. Colloid Interface Sci. 57, 564 (1976).
[12]A. B. Pluchino and S. Arnold (unpublished).
[13]J. C. Maxwell, Philos. Trans. R. Soc. London 170, 231 (1879).
[14]D. V. Derjaguin and Yu. I. Yalamov, in *International Reviews in Aerosol Physics and Chemistry,* edited by G. M. Hidy and J. R. Brock (Pergamon, New York, 1972), Vol. 3, Pt. 2.
[15]H. C. Van de Hulst, *Light Scattering by Small Particles* (Wiley, New York, 1957), pp. 119–124.
[16]P. B. Johnson and R. W. Christy, Phys. Rev. B 6, 4370 (1972).
[17]W. G. Spitzer, D. Kleinman, and D. Walsh, Phys. Rev. 113, 127 (1959).
[18]G. Mie, Ann. Phys. (Leipzig) 25, 377 (1908).
[19]Yu. I. Yalamov, V. B. Kutukov, and E. R. Shchukin, J. Eng. Phys. (Engl. Transl.) 30, 648 (1976).
[20]M. Kerker, *The Scattering of Light and Other Electromagnetic Radiation* (Academic, London, 1969), p. 87.
[21]M. Kerker, Planet Space Sci. 29, 127 (1981).
[22]L. D. Reed, J. Aerosol Sci. 8, 123 (1977).
[23]J. R. Brock, J. Colloid Sci. 17, 768 (1962).
[24]G. A. Slack, J. Appl. Phys. 35, 3460 (1964).
[25]P. M. Sherman, J. Colloid Interface Sci. 51, 87 (1975).